Structural Variation in Human Apolipoprotein E3 and E4: Secondary Structure, Tertiary Structure, and Size Distribution

Chi-Yuan Chou,*‡ Yi-Ling Lin,† Yu-Chyi Huang,† Sheh-Yi Sheu,‡‖ Ta-Hsien Lin,§†‖ Huey-Jen Tsay,¶ Gu-Gang Chang,‡§‖ and Ming-Shi Shiao†

*Graduate Institute of Life Sciences, National Defense Medical Center, Taipei 114, Taiwan; †Department of Medical Research and Education, Taipei Veterans General Hospital, Taipei 112, Taiwan; and ‡Faculty of Life Sciences, §Institute of Biochemistry, ¶Institute of Neuroscience, and ‖Structural Biology Program, National Yang-Ming University, Taipei 112, Taiwan

ABSTRACT Human apolipoprotein E (apoE) is a 299-amino-acid protein with a molecular weight of 34 kDa. The difference between the apoE3 and apoE4 isoforms is a single residue substitution involving a Cys-Arg replacement at residue 112. ApoE4 is positively associated with atherosclerosis and late-onset and sporadic Alzheimer's disease (AD). ApoE4 and its C-terminal truncated fragments have been found in the senile plaques and neurofibrillary tangles in the brain of AD patients. However, detail structural information regarding isoform and domain interaction remains poorly understood. We prepared full-length, N-, and C-terminal truncated apoE3 and apoE4 proteins and studied their structural variation. Sedimentation velocity and continuous size distribution analysis using analytical ultracentrifugation revealed apoE3$_{72\text{-}299}$ as consisting of a major species with a sedimentation coefficient of 5.9. ApoE4$_{72\text{-}299}$ showed a wider and more complicated species distribution. Both apoE3 and E4 N-terminal domain (1–191) existed with monomers as the major component together with some tetramer. The oligomerization and aggregation of apoE protein increased when the C-terminal domain (192–271) was incorporated. The structural influence of the C-terminal domain on apoE is to assist self-association with no significant isoform preference. Circular dichroism and fluorescence studies demonstrated that apoE4$_{72\text{-}299}$ possessed a more α-helical structure with more hydrophobic residue exposure. The structural variation of the N-terminal truncated apoE3 and apoE4 protein provides useful information that helps to explain the greater aggregation of the apoE4 isoform and thus has implication for the involvement of apoE4 in AD.

INTRODUCTION

Human apolipoprotein E (apoE) is a 34-kDa protein containing 299 amino acid residues that mediates the binding of very low-density lipoprotein (VLDL) and intermediate-density lipoprotein (IDL) to the low-density lipoprotein (LDL) receptor and to LDL receptor-related protein (Siest et al., 1995; Selkoe, 2001; Van Bockxmeer et al., 1994; Demant et al., 1991; Kao et al., 1995; Dong et al., 1994; Lalazar and Mahley, 1989). There are three major isoforms of human apoE (namely apoE2, apoE3, and apoE4), which are the products of three alleles (ε2, ε3, and ε4) at a single gene locus on chromosome 19q13.2. The most common isoform of apoE is apoE3, which contains cysteine and arginine at positions 112 and 158. Both positions contain cysteine residues in apoE2 and arginine residues in apoE4 (Fig. 1). Strong correlation of ε4 allele with dyslipidemia and coronary heart disease (CHD) has been demonstrated. The estimated CHD odds associated with the ε4 allele is greater than that for any other known genetic abnormality. The association of ε4 allele with CHD remains significantly high in women, and both sexes combined, after adjustment for traditional coronary risk factors and plasma lipids. ApoE4 homozygosity is also a determinant of restenosis after coronary angioplasty (Van Bockxmeer et al., 1994). ApoE-deficient (apoE(−)) mice develop atherosclerosis spontaneously and the severity is enhanced by a high-cholesterol diet.

The apoE4 isoform also contributes to the pathogenesis of Alzheimer's disease (AD; Selkoe, 2001; Schellenberg, 1995; Marx, 1993; Pericak-Vance and Haines, 1995; Strittmatter and Roses, 1995; Polvikoski et al., 1995; Henderson et al., 1995; Huang et al., 2001; Nathan et al., 1994; Sanan et al., 1994; Raffai and Weisgraber, 2003; Chauhan, 2003). The ε4 allele is associated with both familial late-onset and sporadic AD, and the gene dose of ε4 is a major risk factor for the disease. Accumulated apoE is found in the senile plaques and neurofibrillary tangles (NFT) seen on postmortem examination of the brains of AD patients. AD patients who are homozygous for the ε4 allele exhibit more highly developed senile plaques at autopsy. In cultures of dorsal root ganglion neurons, apoE3 increases neurite outgrowth, whereas apoE4 decreases outgrowth (Nathan et al., 1994). ApoE associates with β-amyloid peptides (Aβ) to form novel monofibrils (Sanan et al., 1994). Furthermore, the neuropathology and the apoE profile of aged chimpanzees have implications for

Submitted May 28, 2004, and accepted for publication September 27, 2004.

Address reprint requests to Gu-Gang Chang, Faculty of Life Sciences, National Yang-Ming University, Taipei 112, Taiwan. Tel.: 886-2-2826-7168; Fax: 886-2-2820-2449; E-mail: ggchang@ym.edu.tw; or to Ming-Shi Shiao, Dept. of Medical Research and Education, Taipei Veterans General Hospital, Taipei 112, Taiwan. Tel.: 886-2-2875-1622; Fax: 886-2-2875-1562; E-mail: msshiao@vghtpe.gov.tw.

Abbreviations used: ApoE, apolipoprotein E; Aβ, β-amyloid peptides; AD, Alzheimer's disease; ANS, 1-anilino-8-naphthalenesulfonic acid; apoE(−), ApoE-deficient; CD, circular dichroism; CHD, coronary heart disease; DLS, dynamic light scattering; IDL, intermediate-density lipoprotein; IPTG, isopropyl-1-thio-α-D-galactoside; LDL, low-density lipoprotein; NFT, neurofibrillary tangles; PBS, phosphate buffered saline; PCR, polymerase chain reaction; VLDL, very low-density lipoprotein.

0006-3495/05/01/455/12 $2.00

doi: 10.1529/biophysj.104.046813

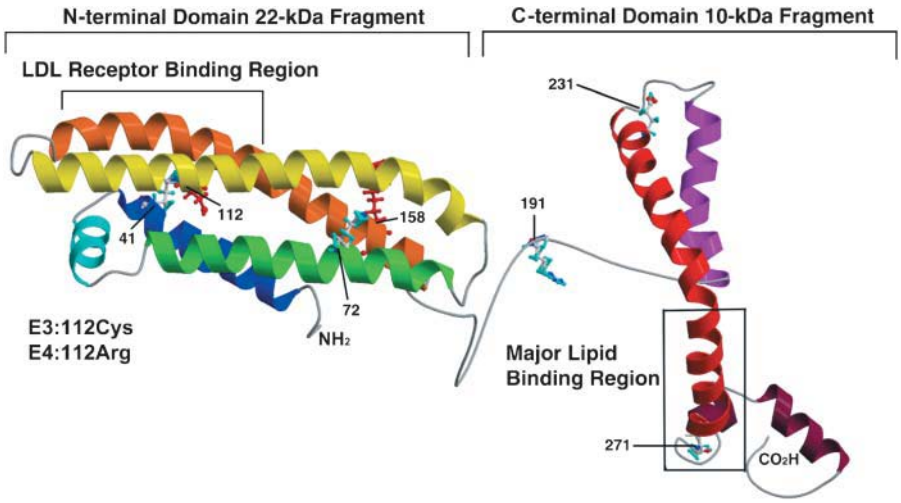

FIGURE 1 Human apolipoprotein E. The model structure illustrates the structural regions where deletions were made (deletion of helix 1, residues 1–40; helices 1 and 2, residues 1–71; C-terminal domain, 192–299; helices 6 and 7, 232–299; and helix 7, 272–299) and also shows the polymorphic site (residue 112) that distinguished apoE3 from apoE4. The structure was modified from apoE299_20K (S. Y. Sheu, unpublished data).

AD (Gearing et al., 1994) and C-terminal truncated apoE4 causes AD-like neurodegeneration and behavioral deficits in transgenic mice (Harris et al., 2003).

Recent evidence has indicated that apoE is folded into two independent structural domains (Dong et al., 1994). Limited thrombolytic digestion provides two large fragments with one fragment corresponding to residues 1–199, a 22-kDa N-terminal domain and the other one to residues 216–299, a 10-kDa C-terminal domain (Fig. 1). Crystallographic studies suggest an amphipathic, extended, and antiparallel four-helix bundle for the N-terminal domain (Wilson et al., 1991). The region of residues 136–158, which is rich in basic amino acids, is involved in LDL receptor binding (Siest et al., 1995). The apoE4 isoform binds preferentially to VLDL and the interaction of Arg-61 with Glu-255 may stabilize an extended helical structure in the carboxyl terminus to accommodate a larger, less-curved VLDL surface (Dong and Weisgraber, 1996). The C-terminal domain of apoE beyond residue 191 contains three predicted helices, namely residues 203–223, 225–266, and 268–289 (Wilson et al., 1991; De Pauw et al., 1997). The end of the second helix may play a key role in lipid binding in apoE and lipoprotein interaction (Westerlund and Weisgraber, 1993; Weisgraber, 1994). The third helix (G* helix) induces the aggregation of C-terminus that becomes monomer after the polar/charged mutation of five residues (Phe-257, Trp-264, Val-269, Leu-279, and Val-287; Fan et al., 2004). Choy et al. (2004) have also shown intermolecular coiled-coil helical formation in the C-terminal domain. The C-terminal region of apoE may also interact with Aβ in forming NFT (Huang et al., 2001). The N-terminal and C-terminal truncated apoE4 proteins have been found to occur in AD brains and induced intracellular NFT-like inclusions in cultured neurons (Huang et al., 2001). However, the structural characters of apoE isoforms that may lead to the differences in molecular pathogenesis of AD remain poorly understood.

To elucidate the structural difference between apoE3 and apoE4, especially with respect to N-terminal and C-terminal truncation, we have expressed full-length and N- or C-terminal-truncated human apoE3 and apoE4 proteins and compared secondary structure, tertiary structure, and quaternary species distribution.

MATERIALS AND METHODS

Plasmids

The pET-29a (+) (Novagen, Madison, WI) vectors used carry a C-terminal His·Tag sequence and multiple cloning sites beyond the f1 origin. This kanamycin-resistant vector was transformed into the BL21 (DE3) strain of *Escherichia coli*. The expression of protein was induced with 1.0 mM isopropyl-1-thio-β-D-galactoside (IPTG) and the cells were harvested at 18°C for overnight or 37°C for 3–5 h.

Construction of human apoE3 expression vectors

The human apoE3 cDNA fragments were first amplified by PCR and ligated into pGEM-T vector (Promega, Madison, WI). The forward primer was 5′-CATATGAAGGTGGAGCAAGCGGTG, and the reverse primer was 5′-GCTCGAGTGATTGTCGCTGGGCACA. The apoE3 cDNA-carried T vectors were then digested with *Nde*I and *Xho*I. Finally, the 0.9-kb fragment end product was ligated to the 5.2-kb *Nde*I-*Xho*I fragment from pET-29a (+). This in turn resulted in a 6.1-kb pET-apoE3 vector, in which apoE3 cDNA was driven by the T7 promoter and the protein was C-terminally fused to a His·Tag sequence (Ser^2-His^6).

Construction of N-terminal or C-terminal truncated apoE3 expression vectors

The pET-apoE3 vector was used as the template. The $apoE3_{41\text{-}299}$, $apoE3_{72\text{-}299}$, $apoE3_{1\text{-}191}$, $apoE3_{1\text{-}231}$, and $apoE3_{1\text{-}271}$ cDNA fragments were amplified by PCR and ligated into pGEM-T vector (Promega). For $apoE3_{41\text{-}299}$, the forward primer was 5′-CATATGCAGACACTGTCTGAGCAGG and for $apoE3_{72\text{-}299}$, 5′-CATATGAAGGCCTACAAATCGGAACT. The reverse primer for $apoE3_{41\text{-}299}$ and $apoE3_{72\text{-}299}$ was

5′-CTCGAGGTGATTGTCGCTGGGCACA. The forward primer for apoE3$_{1\text{-}191}$, apoE3$_{1\text{-}231}$, and apoE3$_{1\text{-}271}$ was 5′-TATACATATGAAGGTG-GAGCAAG. The reverse primer for apoE3$_{1\text{-}191}$ was 5′-AACTCGAGCCG-CACGCGGC; for apoE3$_{1\text{-}231}$, 5′-AACTCGAGCTCGTCCAGGCGG; and for apoE3$_{1\text{-}271}$, 5′-AACTCGAGGTCTTCCACCAGGG. After digesting with *Nde*I and *Xho*I, the cDNA fragment end products were ligated to the 5.2-kb *Nde*I-*Xho*I fragment from pET-29a (+).

Construction of human apoE4 expression vectors

Site-directed mutagenesis (Braman et al., 1996) was used to construct pET-apoE4, pET-apoE4$_{41\text{-}299}$, pET-apoE4$_{72\text{-}299}$, pET-apoE4$_{1\text{-}191}$, pET-apoE4$_{1\text{-}231}$, and pET-apoE4$_{1\text{-}271}$ vectors. The forward primer was 5′-GAGGACGTGCGCGGCCGCCTG and the reverse primer was 5′-AGG-CGGCCGCGCACGTCCTCC. Briefly, pET-apoE3, pET-apoE3$_{41\text{-}299}$, pET-apoE3$_{72\text{-}299}$, pET-apoE3$_{1\text{-}191}$, pET-apoE3$_{1\text{-}231}$, and pET-apoE3$_{1\text{-}271}$ vectors were used as templates and the desired primers were used to mutate the Cys-112 codon to the Arg-112 codon by PCR using *Pfu* DNA polymerase (Promega). After 16–18 temperature cycles, mutated plasmid containing staggered nicks were generated. The PCR products were then treated with *Dpn*I (New England Biolabs, Beverly, MA) to digest the pET-apoE3 templates. Finally, the nicked vector DNA incorporating the desired mutations was transformed into *E. coli* and their DNA sequence was checked by autosequencing.

Purification of the full-length, N-terminal, and C-terminal truncated apoE proteins

After induced by IPTG at 18°C overnight (apoE full-length, apoE$_{1\text{-}191}$, apoE$_{1\text{-}231}$, and apoE$_{1\text{-}271}$) or 37°C for 3–5 h (apoE$_{41\text{-}299}$ and apoE$_{72\text{-}299}$), the cells were centrifuged at 6000 × *g* at 4°C for 10 min. The supernatant was removed and the cell pellets were again suspended in the binding buffer (4 mM imidazole, 300 mM sodium chloride, and 20 mM Tris-HCl, pH 7.9). The cells were sonicated by 60 10-s bursts at 300 W with a 10-s cooling period between each burst. The lysate was centrifuged at 10,000 × *g* for 25 min at 4°C to pellet the cellular debris. One milliliter of the 50% Ni-NTA slurry was equilibrated with the binding buffer and then added to the cleared lysate and the solution mixed gently at 4°C for 60 min. The lysate-Ni-NTA mixture was loaded into a column and washed with the washing buffer (40 mM imidazole, 300 mM sodium chloride, and 20 mM Tris-HCl, pH 7.9). Finally, apoE proteins were eluted with the elution buffer (400 mM imidazole, 300 mM sodium chloride, and 20 mM Tris-HCl, pH 7.9). The purity of all recombinant proteins was estimated to be >95% by the SDS-PAGE. The molar masses of the purified apoE3 and apoE4 proteins (35,365 and 35,418 Da, respectively) were determined by electrospray mass spectrometry and agreed with the theoretical values. The molecular weights of apoE$_{41\text{-}299}$, apoE$_{72\text{-}299}$, apoE$_{1\text{-}191}$, apoE$_{1\text{-}231}$, and apoE$_{1\text{-}271}$, were 30, 27, 23, 28, and 33 kDa, respectively, as anticipated (Fig. 2). Typical yields of the full-length apoE3 and apoE4 proteins were 1.0 mg/l and those of apoE3 and apoE4 N- or C-terminal truncated proteins were 5.0 mg/l after purification.

Buffer change

The purified proteins were concentrated by Amicon Ultra-4 centrifugal filter devices (Millipore, Billerica, MA) with molecular weight cutoff at 10 kDa. The purified proteins were concentrated to 5–10 mg/ml and diluted to 0.5–1.0 mg/ml by PBS (4 mM monosodium dihydrogen phosphate, 16 mM disodium monohydrogen phosphate, and 150 mM sodium chloride, pH 7.3). The result was that after repeating the concentration-dilution procedure five times, the elution buffer had been fully replaced.

Sedimentation velocity

Sedimentation velocity experiments were performed using a Beckman model XL-A analytical ultracentrifuge (Fullerton, CA). Before experiments, samples in PBS buffer were diluted to 0.15, 0.50, or 1.00 mg/ml. Samples (400 μl) and reference (440 μl) solutions were loaded into double-sector centerpieces and mounted in a Beckman An-50 Ti rotor. Experiments were performed at 20°C with a rotor speed of 40,000 rpm. Absorbance of the sample at 280 nm was monitored in a continuous mode, time interval of 480 s, and a step size of 0.002 cm without averaging. Multiple scans at different time points were fitted to a continuous size distribution (see below) by using the program SEDFIT (Schuck, 2000; Schuck et al., 2002) (http://www.analyticalultracentrifugation. com/download.htm) and to a monomer-tetramer rapid self-association model (see below) by using the program SEDPHAT (Schuck, 2003) (http://www.analyticalultracentrifugation.com/sedphat/sedphat.htm). To evaluate the weight-average sedimentation coefficients (s_w), the following equation, which was modified from Fujita (1975) and Baldwin (1953), was used (Eq. 1).

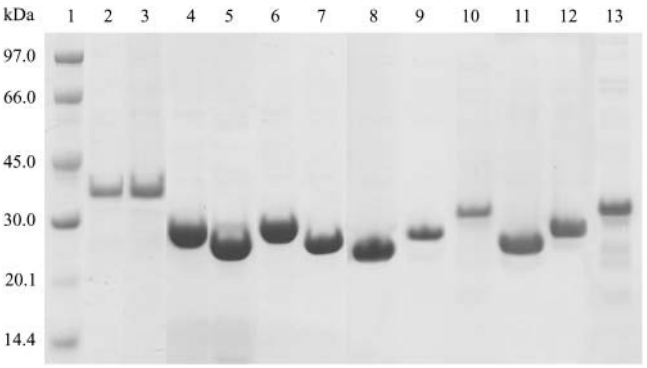

FIGURE 2 SDS-PAGE analysis of the recombinant human apolipoprotein E. Proteins were analyzed on a gradient (4–12%) gel and stained with Coomassie blue. Lane 1, molecular mass markers; lane 2, apoE3; lane 3, apoE4; lane 4, apoE3$_{41\text{-}299}$; lane 5, apoE3$_{72\text{-}299}$; lane 6, apoE4$_{41\text{-}299}$; lane 7, apoE4$_{72\text{-}299}$; lane 8, apoE3$_{1\text{-}191}$; lane 9, apoE3$_{1\text{-}231}$; lane 10, apoE3$_{1\text{-}271}$; lane 11, apoE4$_{1\text{-}191}$; lane 12, apoE4$_{1\text{-}231}$; lane 13, apoE4$_{1\text{-}271}$.

$$s_w(c_p) = -1/2\omega^2 \times d/dt \times log[1 - 2/c_0 r_p^2 \int (c_0 - c(r,t))rdr], \quad (1)$$

in which $s_w(c_p)$ is the weight-average sedimentation coefficient at the plateau concentration c_p and r_p, the plateau radius value. The program SEDFIT containing this equation was used for calculating s_w (Schuck, 2003).

Continuous size distribution analysis

The continuous size (mass or sedimentation coefficient) distribution of the proteins can be determined by using finite element solutions of the Lamm equation combined with size distribution analysis techniques by regularization (Schuck, 2000; Schuck et al., 2002). In brief, the observed sedimentation profiles are described as a superimposition of the contributions of each subpopulation $c(s)$ of particles with sedimentation coefficients between s and $s + ds$ by the integral equation (Eq. 2).

$$a(r,t) \cong \int c(s)L(s,D,r,t)ds, \quad (2)$$

where $a(r,t)$ represents the experimentally observed signal at radius r and time t. $L(s,D,r,t)$ denotes the sedimentation profile of an ideally sedimenting monodisperse species of sedimentation coefficient s and diffusion constant D, calculated as the solution to the Lamm equation (Lamm, 1929). Similarly, the size distribution can be calculated as a molar mass distribution, $c(M)$, according to Eq. 3.

$$a(r,t) \cong \int c(M)L(M,D,r,t)dM. \quad (3)$$

The distributions were calculated using maximum entropy regularization, selecting the most parsimonious distribution within a predefined confidence level p for the quality of fit. An average anhydrous ratio (f/f_0) representing the ratio of frictional coefficient to that of an anhydrous sphere was employed, together with the Stokes-Einstein and the Svedberg equation, for estimating the diffusion coefficient D for all species (Schuck, 2000). All size distributions were solved on a confidence level of $p = 0.95$ or 0.68, a best fitted f/f_0, and a resolution N of 250 sedimentation coefficients between 0.1 and 25.0 S or molar mass between 1 and 1000 kDa, respectively.

Monomer-tetramer rapid self association model analysis

For rapidly associating systems, finite element solutions of the Lamm equation

$$\partial c/\partial t = -1/r(\partial/\partial r(s_w(c(r))\omega^2 r^2 c - D_g(c(r))r\partial c/\partial r)), \quad (4)$$

with local weight-average sedimentation coefficients s_w and gradient-average diffusion coefficients D_g were calculated as described previously (Schuck, 2003, 1998; Cox, 1969). For Lamm equation solutions with hydrodynamic repulsive nonideality, the local weight-average sedimentation coefficients were multiplied with a factor of $1/(1 + k_s c_{tot}(r))$, as described previously (Solovyova et al., 2001).

Dynamic light scattering

The dynamic light scattering (DLS) experiment was performed using a Proterion Protein Solution (Piscataway, NJ) DynaPro-MS/X dynamic light-scattering instrument. The laser power was set 20%, acquisition time was 10 s, and the temperature was 20°C. Intensity, contents, hydrodynamic radius (R), and polydispersity of the protein sample in PBS (pH 7.3) were real-time detected and analyzed by the software Dynamics V6. The total detecting time of each sample was 30–40 min.

Circular dichroism spectrometry

Circular dichroism (CD) spectrometry was performed using a Jasco J-810 spectropolarimeter (Easton, MD). Spectra of the sample dissolved in PBS (pH 7.3) were recorded at 30°C using 0.01-cm quartz cuvettes with a wavelength range of 190–250 nm at a step size of 0.2 nm. Signal averaging time was 1.0 s, and the slit bandwidth was 2 nm. The mean residue ellipticity ([Θ]) at each wavelength was calculated from Eq. 5,

$$[\Theta] = MRW \times \theta_\lambda / 10 \times l \times c, \quad (5)$$

where MRW is the mean residue weight, θ_λ is the measured ellipticity in degree at wavelength λ, l is the cuvette pathlength (0.01 cm), and c is the protein concentration in g/ml. The deconvolution was performed using online CD analysis by DICHROWEB (Lobley and Wallace, 2001; Lobley et al., 2002) (http://www.cryst.bbk.ac.uk/cdweb/html/home.html). DICHROWEB offers several important pieces of analysis software for secondary structure determination, such as CONTINLL (Provencher and Glockner, 1981; Van Stokkum et al., 1990), SELCON3 (Sreerama and Woody, 1993; Sreerama et al., 1999), and K2D (Andrade et al., 1993).

ANS fluorescence spectrometry

Fluorescent dye binding experiments with 1-anilino-8-naphthalenesulfonic acid (ANS) as a probe were performed using Perkin-Elmer LS 50B luminescence spectrometer (Foster City, CA). The fluorescence emission of ANS is known to increase upon binding to accessible hydrophobic region of a protein (Semisotnov et al., 1991; Rogers et al., 1997). A fixed concentration of ANS (250 μM) was mixed with the protein (3 μM) in PBS (pH 7.3). The excitation wavelength was set at 395 nm and the emission spectrum was monitored from 400 to 600 nm wavelength. The area of the spectrum was calculated by the peak-fitting module of the Origin program (OriginLab, Northampton, MA). The average emission wavelength, $\langle\lambda\rangle$, was calculated using Eq. 6,

$$\langle\lambda\rangle = \Sigma(F \times \lambda)/\Sigma F, \quad (6)$$

where F is the fluorescence intensity and λ is the wavelength (Sánchez del Pino and Fersht, 1997).

RESULTS

Hydrodynamic behaviors and s_w of apolipoprotein E3 and E4 by sedimentation velocity

The sedimentation boundary of the sedimentation velocity data of 0.50 mg/ml of apoE3 protein at 480-s intervals is shown in Fig. 3. The open circles in Fig. 3 *A* represent the experimental data and solid lines represent the best-fit sedimentation profiles to a continuous size distribution analyzed by SEDFIT. The grayscale of residual bitmap and random distribution of residuals (Fig. 3, *B* and *C*), respectively, both show a high quality of fit. In the fitting process, maximum entropy regularization ($p = 0.95$ or 0.68) and resolution of $n = 250$ were used according to Schuck (2000). The fitting results are shown as calculated $c(s)$ versus sedimentation coefficient (Fig. 3, *D* and *E*) or calculated $c(M)$ versus mass (Fig. 3 *F*). The distribution of each species was more clearly defined when a regularization of $p = 0.68$ was used (Fig. 3 *E*). ApoE4 and the other truncated fragments at different protein concentrations (0.15–1.00 mg/ml) were also analyzed (Table 1). Depending on the sequence and size of proteins, the partial specific volume of all the proteins was calculated (~0.73 ml/g) by program SEDNTERP (Laue et al., 1992) and so were molar extinction coefficients. Root mean square deviation (rmsd) of fitting to the continuous size distribution model was from 0.00384 to 0.00773 (Table 1). According to Schuck (2000) and Schuck et al. (2002), the fit in our studies was good and showed a high quality ($rmsd < 0.01$). Every sedimentation velocity experiment was repeated twice and similar results were obtained.

The s_w value was calculated by second moment integration (Schuck, 2003; Table 1). The s_w values of apoE and $apoE_{1\text{-}271}$ proteins were from 6.1 to 6.6 S and did not show any significant difference. The C-terminal truncated $apoE_{1\text{-}191}$ showed the lowest s_w (2.6–3.0 S), whereas $apoE3_{1\text{-}231}$ had an s_w of 3.8–4.2 S and $apoE4_{1\text{-}231}$ had an s_w of 3.1–3.6 S. $ApoE3_{41\text{-}299}$ and $apoE4_{41\text{-}299}$ proteins showed lower s_w values (4.4 and 3.7 S) at 0.15 mg/ml and higher s_w values (4.8 and 4.3 S) at 0.50 or 1.00 mg/ml, respectively. Finally, the s_w of the $apoE4_{72\text{-}299}$ protein had significantly increased (from 6.4 to 7.2) at a higher protein concentration, but $apoE3_{72\text{-}299}$ did not.

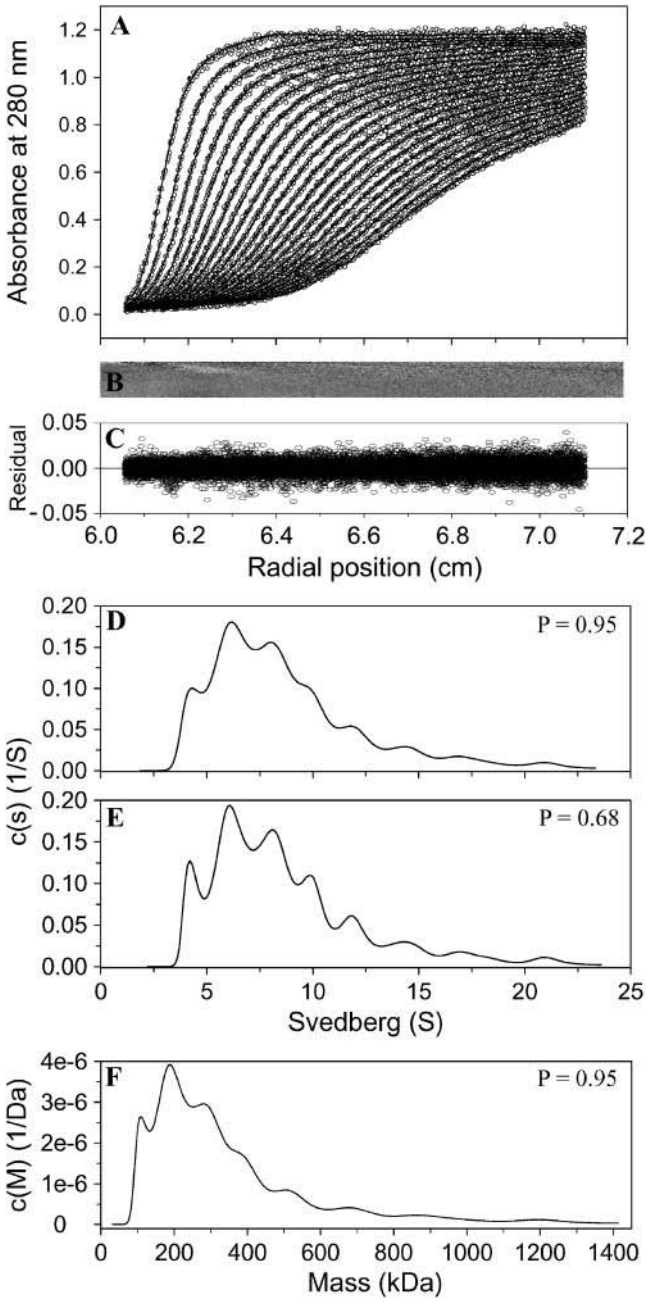

FIGURE 3 Sedimentation velocity experiments of apoE3. A fixed initial protein concentration at 0.50 mg/ml was used for the proteins. Analytical ultracentrifugation was performed at a rotor speed of 40,000 rpm, rotor temperature of 20°C in PBS (pH 7.3), and A_{280nm} was scanned. The radial data collecting interval was 0.002 cm and time interval of scans was 480 s. (*A*) Circles represent the observed spectrum and solid lines are computer-generated results by fitting the experimental data to the Lamm equation with the SEDFIT program. (*B*) Grayscale of residual bitmap. (*C*) Residuals plotted as a function of radial position. (*D* and *E*) Continuous sedimentation coefficients distribution of the apoE3 proteins at the regularization of $p = 0.95$ and 0.68. (*F*) Continuous molar mass distribution of the apoE3 protein at the regularization of $p = 0.95$.

TABLE 1 Sedimentation analysis of full-length and N-terminal truncated apoE3 and apoE4 proteins

	Concentration (mg/ml)	RMSD*	s_w† (S)
ApoE3	0.15	0.00523	6.6
	0.50	0.00746	6.5
ApoE4	0.15	0.00532	6.3
	0.50	0.00743	6.5
$ApoE3_{41-299}$	0.15	0.00391	4.4
	0.50	0.00502	4.9
	1.00	0.00695	4.8
$ApoE4_{41-299}$	0.15	0.00384	3.7
	0.50	0.00504	4.3
	1.00	0.00773	4.3
$ApoE3_{72-299}$	0.15	0.00509	5.5
	0.50	0.00537	5.7
	1.00	0.00726	5.8
$ApoE4_{72-299}$	0.15	0.00413	6.4
	0.50	0.00469	6.9
	1.00	0.00726	7.2
$ApoE3_{1-191}$	0.15	0.00556	2.6
	0.50	0.00654	2.9
$ApoE4_{1-191}$	0.15	0.00605	2.7
	0.50	0.00713	3.0
$ApoE3_{1-231}$	0.15	0.00546	3.8
	0.50	0.00660	4.2
$ApoE4_{1-231}$	0.15	0.00619	3.1
	0.50	0.00772	3.6
$ApoE3_{1-271}$	0.15	0.00586	6.6
	0.50	0.00740	6.3
$ApoE4_{1-271}$	0.15	0.00588	6.1
	0.50	0.00728	6.1

*RMSD of best fit to continuous $c(s)$ distribution model with $p = 0.95$.
†s_w calculated by second moment integration (Schuck, 2003).

Size distribution of full-length apoE3 and apoE4 proteins

Size distribution of apoE3 and apoE4 full-length proteins showed very similar patterns (Fig. 4, *A* and *B*). Fitting to the continuous size distribution model showed overlapping peaks. To estimate each contributing component, the percentage and s_w of the distribution curve by different integral range were analyzed with the integral function of SEDFIT (Table 2). There were four major species below $s = 10$. The large components ($s > 10$), with their lower content and broad distribution, were calculated as a single region. Both apoE3 and apoE4 proteins were separated into a five region distribution. The distribution of these components was very similar for both protein concentrations (0.15 mg/ml and 0.50 mg/ml). Concentration-dependent variation was observed. The aggregation species corresponding to $s = 15.1$ of apoE3 showed 6% increase and the species at $s = 7.9$ increased by 5%, whereas the smaller species at $s = 4.0$ and 5.9 showed 11% decreases. A similar trend was also observed in apoE4 species corresponding to $s = 7.8$, 9.8, and 14.9, which increased by 23% and those of $s = 3.9$ and 5.8, which decreased by 23%. Furthermore, at higher protein concentration, large species ($s > 10$) were more significantly increased for the apoE4 protein (by 15%), compared to

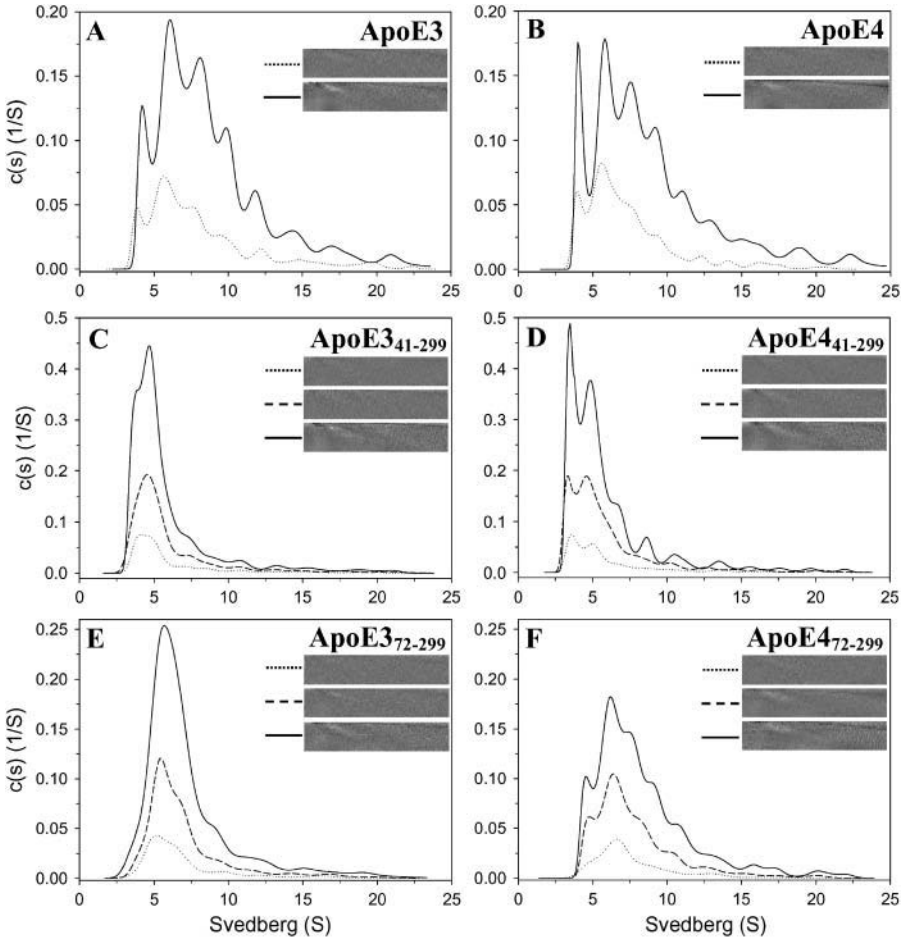

FIGURE 4 Continuous distribution analysis of the apoE3 (*A*), apoE4 (*B*), apoE3$_{41-299}$ (*C*), apoE4$_{41-299}$ (*D*), apoE3$_{72-299}$ (*E*), and apoE4$_{72-299}$ proteins (*F*) at different concentrations. Experiments were conducted at an initial protein concentration of 0.15 (*dotted line*), 0.50 mg/ml (*A* and *B*, *solid line*; *C–F*, *dashed line*), or 1.00 mg/ml (*solid line*) in PBS (pH 7.3) at 20°C, rotor speed 40,000 rpm. Data were collected at time intervals of 480 s. The confidence level of the regularization after fitting was $p = 0.68$. (*Insets*) Grayscale of residual bitmap.

apoE3 protein (6%). These observations support the greater aggregation of apoE4 protein.

Size distribution of N-terminal truncated apoE3 and apoE4 proteins

Fig. 4, *C* and *D*, shows the best-fit continuous $c(s)$ distribution of apoE3$_{41-299}$ and apoE4$_{41-299}$ proteins. In size distribution from $s = 2.5–6.5$ at $p = 0.55$ (data not shown), both apoE$_{41-299}$ proteins showed two major species of s = 3.6–3.9 and 5.0–5.1. After calculating the integration by SEDFIT, five species were identified for both apoE$_{41-299}$ proteins (Table 2). At an initial protein concentration of 1.00 mg/ml, the major species of apoE3$_{41-299}$ with $s = 3.7$ and 5.0 accounted for 77% of the total amount. In the case of apoE4$_{41-299}$, the major species with $s = 3.6$ and 5.1 constituted 72% of the total protein amount. Like those of full-length apoE proteins, protein concentration influenced the percentage of some species. In apoE3$_{41-299}$ protein, the percentage of $s = 3.9$ decreased by 16% and that of $s = 5.1$ increased by 17% when the protein concentration was increased from 0.15 to 1.00 mg/ml. ApoE4$_{41-299}$ showed a 7% decrease in $s = 3.7$ and 8% increase in $s = 5.1$ at higher protein concentrations. However, both apoE$_{41-299}$ proteins showed less large species of $s > 10$ (decreased 1–4%). Neither apoE3$_{41-299}$ nor apoE4$_{41-299}$ therefore showed a tendency to aggregate.

Fig. 4, *E* and *F*, shows the best-fit continuous $c(s)$ distribution of apoE3$_{72-299}$ and apoE4$_{72-299}$. ApoE4$_{72-299}$ (Fig. 4 *F*) showed a more complicated distribution pattern than apoE3$_{72-299}$ (Fig. 4 *F*). The protein concentration had a significant influence on the distribution of species in apoE4$_{72-299}$ solution. The major species in apoE3$_{72-299}$ was $s = 5.9$ at 1.00 mg/ml protein concentration, whereas those in apoE4$_{72-299}$ were overlapping peaks separated into five species: $s = 4.5$, 6.1, 7.7, 9.3, and 11.0 (Fig. 4 *F*). After calculating the integration by SEDFIT, both apoE$_{72-299}$ proteins showed four species at 0.15 mg/ml protein concentration (Table 2). However, when the protein concentration was increased to 1.00 mg/ml, 10 species were found in apoE4$_{72-299}$ protein, compared with five species of apoE3$_{72-299}$ (Fig. 4, *E* and *F*). This feature showed that aggregation of apoE4$_{72-299}$ protein was more sensitive to concentration. The smallest apoE4$_{72-299}$ species with $s = 4.6$ decreased by 4% at the higher protein concentration. At the same time, species $s = 6.6$ and 9.4 decreased by 24 and 8%, respectively, species $s = 7.7$ remained at 23%, and those with $s > 10$ increased by 14%. Similar to the full-length

TABLE 2 Size distribution analysis of full-length and N-terminal truncated apoE3 and apoE4 proteins by serial integration

	0.15 mg/ml			1.00 mg/ml*		
Concentration	Integral range[†] (S)	s_w[‡] (S)	Integral area	Integral range (S)	s_w (S)	Integral area
ApoE3	2.5–4.5	4.0 ± 0.4	0.05 (13%)[§]	3.4–4.9	4.3 ± 0.3	0.12 (10%)
	4.5–7.1	5.9 ± 0.7	0.15 (38%)	4.9–7.2	6.1 ± 0.6	0.34 (30%)
	7.1–9.0	7.9 ± 0.5	0.08 (21%)	7.2–9.3	8.2 ± 0.6	0.30 (26%)
	9.0–11.2	9.9 ± 0.6	0.05 (13%)	9.3–11.0	10.0 ± 0.5	0.15 (13%)
	11.2–23.9	15.1 ± 3.1	0.06 (15%)	11.0–23.1	14.6 ± 3.1	0.24 (21%)
ApoE4	2.7–4.4	3.9 ± 0.3	0.05 (13%)	3.2–4.7	4.1 ± 0.3	0.12 (11%)
	4.4–7.1	5.8 ± 0.7	0.17 (45%)	4.7–6.7	5.8 ± 0.5	0.25 (24%)
	7.1–8.8	7.8 ± 0.5	0.07 (18%)	6.7–8.5	7.6 ± 0.5	0.24 (23%)
	8.8–11.5	9.8 ± 0.7	0.05 (13%)	8.5–10.4	9.4 ± 0.5	0.17 (16%)
	11.5–23.4	14.9 ± 2.6	0.04 (11%)	10.4–24.4	14.6 ± 3.5	0.28 (26%)
$ApoE3_{41-299}$	2.8–4.5	3.9 ± 0.3	0.08 (38%)	2.8–4.1	3.7 ± 0.3	0.28 (22%)
	4.5–6.3	5.1 ± 0.5	0.08 (38%)	4.1–6.5	5.0 ± 0.6	0.70 (55%)
	6.3–8.0	7.1 ± 0.5	0.02 (9%)	6.5–8.1	7.2 ± 0.5	0.12 (9%)
	8.0–9.7	8.7 ± 0.5	0.01 (5%)	8.1–9.9	8.9 ± 0.5	0.06 (5%)
	9.7–22.3	13.9 ± 3.3	0.02 (10%)	9.9–22.8	14.2 ± 3.3	0.12 (9%)
$ApoE4_{41-299}$	2.5–4.4	3.7 ± 0.4	0.08 (38%)	2.5–4.2	3.6 ± 0.3	0.42 (31%)
	4.4–6.1	5.1 ± 0.4	0.07 (33%)	4.2–6.2	5.1 ± 0.5	0.55 (41%)
	6.1–7.5	6.7 ± 0.4	0.02 (10%)	6.2–7.7	6.8 ± 0.4	0.16 (12%)
	7.5–9.2	8.3 ± 0.5	0.01 (5%)	7.7–9.6	8.6 ± 0.5	0.08 (6%)
	9.2–21.5	13.4 ± 3.4	0.03 (14%)	9.6–22.9	13.7 ± 3.4	0.14 (10%)
$ApoE3_{72-299}$	1.5–5.9	4.9 ± 0.6	0.07 (47%)	1.7–8.2	5.9 ± 1.1	0.72 (77%)
	5.9–8.5	6.8 ± 0.7	0.05 (33%)	8.2–10.3	9.1 ± 0.6	0.10 (11%)
	8.5–11.0	9.6 ± 0.7	0.01 (7%)	10.3–22.8	14.0 ± 3.1	0.11 (12%)
	11.0–20.8	14.4 ± 2.5	0.02 (13%)			
$ApoE4_{72-299}$	3.0–5.2	4.6 ± 0.5	0.02 (14%)	3.6–5.0	4.5 ± 0.3	0.09 (10%)
	5.2–8.1	6.6 ± 0.8	0.08 (57%)	5.0–7.0	6.1 ± 0.5	0.30 (33%)
	8.1–11.7	9.4 ± 1.0	0.03 (21%)	7.0–8.6	7.7 ± 0.5	0.21 (23%)
	11.7–20.1	13.9 ± 1.9	0.01 (7%)	8.6–10.1	9.3 ± 0.4	0.12 (13%)
				10.1–23.6	13.5 ± 3.1	0.19 (21%)

*Full-length apoE3 and apoE4 proteins were at 0.50 mg/ml.
[†]Sedimentation coefficient of continuous $c(s)$ distribution model by SEDFIT (Schuck, 2000). The distributions were regularized by maximum entropy with 0.68 confidence level.
[‡]Weight-average sedimentation coefficients calculated by SEDFIT.
[§]The area in different integral range was calculated by SEDFIT and values in parentheses were the area percentage.

proteins, at higher protein concentrations, $apoE4_{72-299}$ had more abundant larger species ($s > 10$, 21%), compared with those of $apoE3_{72-299}$ (12%). $ApoE4_{72-299}$ therefore shows a greater tendency to aggregate.

Size distribution of C-terminal truncated apoE3 and apoE4 proteins

Fig. 5, *A* and *C*, shows the best-fit continuous $c(s)$ distribution of the C-terminal truncated apoE proteins. At the initial protein concentration of 0.15 mg/ml, both $apoE3_{1-191}$ and $apoE4_{1-191}$ existed as two major peaks with $s = 2.1$ and $s = 4.5$ values (*solid lines* in Fig. 5, *A* and *C*). The two-species distribution was still maintained in the case of the $apoE3_{1-231}$ and $apoE4_{1-231}$ (*dashed lines* in Fig. 5, *A* and *C*), whereas the s values were shifted to 2.4 and 5.5 and the ratio of the two species also changed. From the results of $c(M)$ distribution, the mass of the two species were estimated to be ~22 kDa and 85 kDa for $apoE_{1-191}$ and ~30–35 kDa and 110–140 kDa for $apoE_{1-231}$ (Fig. 5, *B* and *D*). These two species were assumed to be monomer and tetramer.

To further evaluate the association of monomer and tetramer, the monomer-tetramer rapid self-association model was used to calculate dissociation constants, K_d. The K_d of $apoE3_{1-191}$ (556 ± 233 nM) was 19 times larger than that of $apoE3_{1-231}$ (29 ± 2.8 nM) and 37 times in the case of apoE4 isoforms (592 ± 323 nM of $apoE4_{1-191}$ and 16 ± 1.3 nM of $apoE4_{1-231}$). Both $apoE3_{1-231}$ and $apoE4_{1-231}$ showed greater tendency toward tetramerization.

Different from the 1–191 and 1–231 fragments in size distribution, $apoE_{1-271}$ proteins showed overlapping peaks (*dotted lines* in Fig. 5, *A* and *C*). After calculating the integration area by SEDFIT, $apoE3_{1-271}$ could be resolved into six species with $s = 3.6$ (8%), 6.4 (64%), 8.9 (16%), 10.8 (8%), 13.2 (4%), and 17.4 (1%). The protein $apoE4_{1-271}$ showed a similar pattern with $s = 3.5$ (4%), 5.6 (29%), 7.0 (29%), 8.4 (17%), 10.2 (13%), 13.2 (4%), and 17.3 (4%), but it should be noted that there was a change in the relative amounts of each species. Similar to the $c(S)$ distribution, continuous $c(M)$ distribution (*dotted lines* in Fig. 5, *B* and *D*) also showed overlapping peaks in the range of 50–400 kDa. $ApoE4_{1-271}$ was made up of more and larger species ($s > 10$;

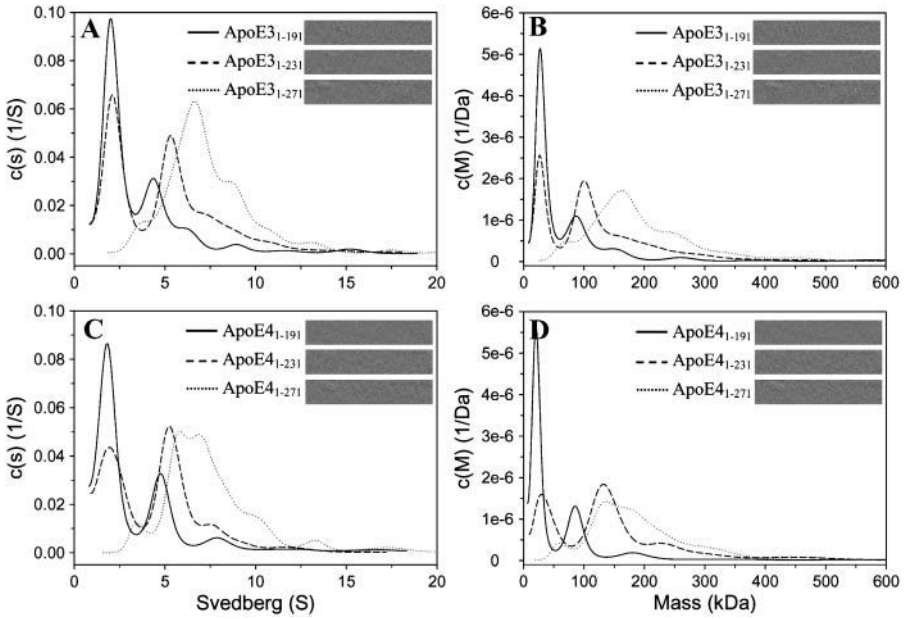

FIGURE 5 Continuous distribution analysis of C-terminal truncated apoE3 (*A* and *B*) and apoE4 fragments (*C* and *D*). Experiments were conducted in PBS (pH 7.3) at 20°C, rotor speed 40,000 rpm. The left panels, continuous sedimentation coefficient distribution, $c(s)$, and the right panels, continuous molar mass distribution, $c(M)$, of the truncated apoE3 and apoE4 proteins (0.15 mg/ml). Solid lines, apoE$_{1-191}$; dashed lines, apoE$_{1-231}$; and dotted lines, apoE$_{1-271}$. The confidence level of the regularization for 1–191 and 1–231 fragments was 0.95 and for 1–271 was 0.68. (*Insets*) Grayscale of residual bitmap.

21%), compared to apoE3$_{1-271}$ (13%). However, they did not show a significant tendency to aggregate at higher protein concentration (data not shown).

Dynamic light scattering of apoE proteins

To verify the size distribution of the apoE3, apoE4, apoE3$_{72-299}$, and apoE4$_{72-299}$ proteins, DLS experiments were performed at an initial protein concentration of 1.0 mg/ml. Both apoE3 and E4 proteins showed a distribution with two major particle groups, one with a size of 3.9 nm and another in the range of 5.0–15.0 nm. However, apoE3 had less 5.0–15.0 nm group particles (35%), compared with those of apoE4 (46%). ApoE3$_{72-299}$ protein existed as one major particle group in the range of 4–10 nm, whereas apoE4$_{72-299}$ showed two major groups with a particle size of 5.1 nm (62%) and another in the range of 10.0–25.0 nm (36%).

Secondary structures of apoE proteins

Far-ultraviolet CD spectroscopy of apoE proteins is shown in Fig. 6. Comparing the two isoforms, the spectra of full-length apoE (*circle lines* in Fig. 6 *A*), 72–299 (*square lines* in Fig. 6 *A*), and 1–271 (*hexagon lines* in Fig. 6 *B*) fragments showed significant difference. All spectral data were further analyzed by the program CONTIN, SELCON3, and K2D. Because these programs showed similar simulations, only the results of CONTIN were shown in Table 3. ApoE3 protein indicated very high α-helical content (91%), whereas that of apoE4 showed less (71%). The difference can also be found when the apoE3$_{1-271}$ (78%) and apoE4$_{1-271}$ (69%) proteins are compared. The N-terminal truncated fragments, apoE3$_{41-299}$ and apoE4$_{41-299}$ proteins maintained ~54–55% α-helix secondary structure and the percentage of random coil had increased by 13% compared with apoE4 and 38% compared with apoE3. ApoE3$_{72-299}$ protein showed relatively low percentage of α-helical structure (38%), and high percentage of random coil (53%). In contrast, apoE4$_{72-299}$ protein still maintained ~49% α-helix and showed less random coil (47%).

In addition to the apoE$_{1-271}$ proteins, the other C-terminal truncated apoE fragments maintained ~50–60% α-helix and did not show an obvious difference between two isoforms.

ANS binding ability of apoE proteins

The binding of apoE proteins with the hydrophobic dye ANS was studied by fluorescence spectroscopy and the results are shown in Fig. 7. ANS alone displayed very low fluorescence in aqueous buffer (Fig. 7, *dotted lines*) and its fluorescence was significantly enhanced when bound to protein hydrophobic patches. Blue shift in the emission wavelength $\langle\lambda\rangle$ was observed after interaction with hydrophobic sites on proteins (Table 4). In both the apoE3 and apoE4 isoforms, the hydrophobic exposure of apoE$_{41-299}$ proteins was always higher than that of full-length apoE proteins (Fig. 7). In addition, the hydrophobic exposure of the two isoforms did not show a significant difference in the case of the full-length or 41–299 fragments. Although apoE$_{72-299}$ protein had lower hydrophobic exposure (compared with full-length and the 41–299 fragments), the apoE4$_{72-299}$ protein still showed more hydrophobic exposure than apoE3$_{72-299}$ protein (20% increase in fit area; Table 4).

Different from the N-terminal truncated fragments, the C-terminal truncation of the two isoforms did not show significant isoform difference. ApoE$_{1-191}$ protein showed very low hydrophobic exposure (only 35% of full-length apoE) and less blue shift in $\langle\lambda\rangle$ (*triangle lines* in Fig. 7 *B*;

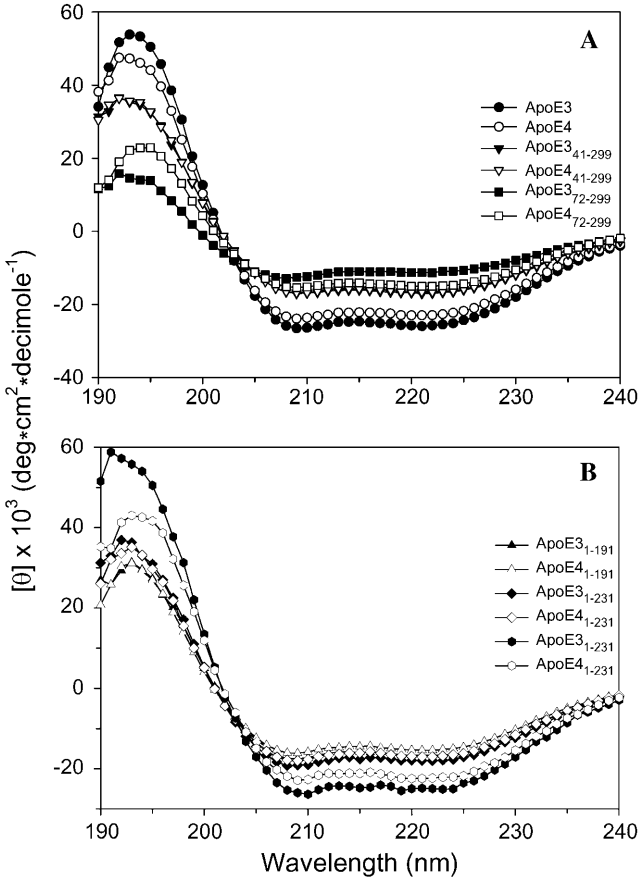

FIGURE 6 CD spectra of full-length and truncated apoE proteins. The spectra were measured in PBS (pH 7.3). In panel *A*, closed circles, apoE3; open circles, apoE4; closed triangles, $apoE3_{41\text{-}299}$; open triangles, $apoE4_{41\text{-}299}$; closed squares, $apoE3_{72\text{-}299}$; open squares, $apoE4_{72\text{-}299}$. In panel *B*, closed triangles, $apoE3_{1\text{-}191}$; open triangles, $apoE4_{1\text{-}191}$; closed diamonds, $apoE3_{1\text{-}231}$; open diamonds, $apoE4_{1\text{-}231}$; closed hexagons, $apoE3_{1\text{-}271}$; open hexagons, $apoE4_{1\text{-}271}$.

Table 4). Compared with $apoE_{1\text{-}191}$ protein, the hydrophobic exposure of $apoE_{1\text{-}231}$ protein showed a large increase (*diamond lines* in Fig. 7 *B*). $ApoE_{1\text{-}271}$ showed the most hydrophobic exposure (*hexagon lines* in Fig. 7 *B*), and fit area had increased by 60%, compared with full-length apoE protein.

DISCUSSION

Structural variations governing the differences in higher-order structures and protein aggregation for apoE3 and apoE4, with only one Cys-Arg substitution at position 112, are most useful for linking apoE isoform structures with the molecular pathogenesis of atherosclerosis and AD. In this study, we purposely truncated the first and second helices in the N-terminal domain of apoE, while maintaining the lipid-interacting C-terminal domain with the aim of examining the roles of helices 1 and 2 in helix stability and domain-domain interactions. In addition, apoE with extensive C-terminal helices truncation was also studied to understand structure variation that may exist in the C-terminus.

TABLE 3 Secondary structures of full-length and truncated apoE3 and apoE4 proteins analyzed by CD spectroscopy

	α-Helix (%)	β-Sheet (%)	Random coil (%)	Normalized RMSD
ApoE3	91.2*	6.9	2.0	0.076
ApoE4	70.9	3.5	25.6	0.052
$ApoE3_{41\text{-}299}$	55.3	5.0	39.6	0.048
$ApoE4_{41\text{-}299}$	56.5	5.0	38.4	0.057
$ApoE3_{72\text{-}299}$	37.6	8.8	53.4	0.048
$ApoE4_{72\text{-}299}$	48.5	5.0	46.5	0.075
$ApoE3_{1\text{-}191}$	53.0	4.5	42.6	0.066
$ApoE4_{1\text{-}191}$	60.1	7.4	32.6	0.091
$ApoE3_{1\text{-}231}$	58.1	4.5	37.4	0.043
$ApoE4_{1\text{-}231}$	56.8	5.0	38.3	0.079
$ApoE3_{1\text{-}271}$	77.7	2.0	20.3	0.030
$ApoE4_{1\text{-}271}$	68.8	2.1	29.0	0.048

*Percentage calculated by CONTIN program (Sreerama et al., 1999).

This study elucidated structural variance between apoE3 and apoE4 isoforms at secondary, tertiary, and quaternary structure levels. ApoE4 showed a higher percentage of randomly coiled structure, compared with apoE3. This may result in a greater tendency to aggregate for apoE4 than apoE3. In the continuous $c(s)$ distribution analyses, full-length apoE3 and apoE4 showed very similar patterns when the initial protein concentration was increased from 0.15 to 0.50 mg/ml. Concentration-dependent variation was observed and large species with $s > 10$ was more significantly increased for apoE4 protein (by 15%), compared with that of apoE3 protein (6%). The distribution patterns were different from those of a previous report (Perugini et al., 2000). However, a higher percent self-association of apoE4 isoform was found and this agrees with the previous report.

When helix 1 only or helices 1 and 2 of the N-terminal domain were truncated, the structural variance of apoE3 and apoE4 became more significant. The size distribution of $apoE3_{41\text{-}299}$ and $apoE4_{41\text{-}299}$ showed minor variance in the percentage of major species, whereas $apoE3_{72\text{-}299}$ and $apoE4_{72\text{-}299}$ showed significant differences in the secondary, tertiary, and quaternary structures. $ApoE4_{72\text{-}299}$ protein maintained more α-helical structure. The accessibility of hydrophobic residues was also higher than for $apoE3_{72\text{-}299}$. These features showed that in addition to the salt bridge between Arg-61 and Glu-255, additional interactions may exist to maintain the structure of $apoE4_{72\text{-}299}$ protein. In addition, $apoE4_{72\text{-}299}$ showed a large amount of aggregation, especially at a high protein concentration. From the DLS experiments, the particle size of $apoE4_{72\text{-}299}$ protein was also larger than that of $apoE3_{72\text{-}299}$. It can be explained by the deletion of Arg-61. . .Glu-255 salt bridge (Dong et al., 1994; Dong and Weisgraber, 1996). Deletion of the N-terminal helices 1 and 2 of apoE3 protein resulted in the loss of most of the secondary structure and yet its major species at $s = 5.9$ was maintained. These observations suggested that the first

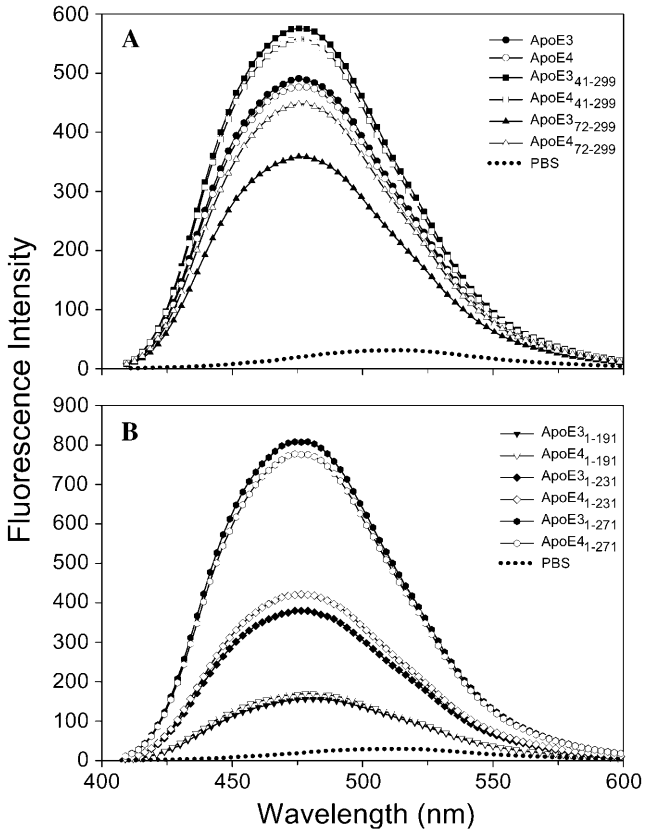

FIGURE 7 Binding of full-length and truncated apoE isoform proteins with ANS as a fluorescence probe. A fixed concentration of ANS (250 μM) and proteins (3 μM) was used. Excitation wavelength was set at 395 nm. The minimum fluorescence of ANS in PBS (pH 7.3) at 25°C was shown by dotted lines. In panel *A*, closed circles, apoE3; open circles, apoE4; closed squares, $apoE3_{41\text{-}299}$; open squares, $apoE4_{41\text{-}299}$; closed triangles, $apoE3_{72\text{-}299}$; open triangles, $apoE4_{72\text{-}299}$. In panel *B*, closed triangles, $apoE3_{1\text{-}191}$; open triangles, $apoE4_{1\text{-}191}$; closed diamonds, $apoE3_{1\text{-}231}$; open diamonds, $apoE4_{1\text{-}231}$; closed hexagons, $apoE3_{1\text{-}271}$; open hexagons, $apoE4_{1\text{-}271}$.

two helices of N-terminal domain may play an important role in the structure stability of apoE3.

Farkas et al. (2004) have showed that the intracellular recycling of apoE and its N-terminal domain in vivo occur via multiple redundant pathways. In addition, Li et al. (2003) have suggested that the receptor 2 binding motif of apoE is localized at the N-terminus. These studies indicate that structural variance in the N-terminal truncated apoE3 and apoE4 may lead to different degradation or recycling pathways. The higher stability of truncated apoE4 proteins may extend the half-life inside or outside the cells, and may further lead to the formation of extracellular aggregated plaques or NFT, the hallmark of AD.

Another point of view was raised by Saito et al. (2001, 2003) and Morrow et al. (2002) and they suggested that the N-terminal domain of apoE4 (residues 1–191) form a molten globule and assume an open or a closed form in the absence or presence of lipid binding, respectively. Change in pH will induce a similar structural change. This phenomenon may be involved in the VLDL-binding efficiency of apoE4 proteins. Our results showed that $apoE4_{72\text{-}299}$ had a higher hydrophobic exposure, suggesting higher lipid-binding affinity, compared to $apoE3_{72\text{-}299}$.

TABLE 4 The ANS fluorescence emission spectrum analysis

Sample*†	Fit area (nm × AU) (× 10^3)	$\langle\lambda\rangle$ (nm)
Buffer only	1.8	512
ApoE3	27.6	485
ApoE4	27.0	485
$ApoE3_{41\text{-}299}$	32.4	485
$ApoE4_{41\text{-}299}$	31.4	485
$ApoE3_{72\text{-}299}$	20.8	486
$ApoE4_{72\text{-}299}$	25.2	486
$ApoE3_{1\text{-}191}$	9.3	490
$ApoE4_{1\text{-}191}$	10.0	489
$ApoE3_{1\text{-}231}$	21.5	486
$ApoE4_{1\text{-}231}$	23.8	486
$ApoE3_{1\text{-}271}$	45.3	485
$ApoE4_{1\text{-}271}$	43.4	485

*Fixed concentration of ANS (250 μM) was used.
†Determination was conducted in PBS at pH 7.3 at 25°C.

The oligomerization of apoE protein is also closely related to the length of its C-terminal domain. From our results, the $apoE_{1\text{-}191}$ protein existed mainly as monomer with some tetramer. When the helix 1 of C-terminal domain remained (192–231), the tetramer content was increased and monomer content was decreased. The $apoE_{1\text{-}271}$ protein showed significant polymerization and the major species were assumed to be tetramers to hexamers (100–200 kDa, Fig. 5, *B* and *D*). Fan et al. (2004) indicated that the G* helix (268–289) is the key motif for the apoE aggregation. Our results suggest that the helices 1 and 2 of C-terminal domain (192–270) also induce polymerization of the apoE and that the K_d of $apoE_{1\text{-}231}$ is significantly decreased and the polymerization of $apoE_{1\text{-}271}$ is significant, as compared to $apoE_{1\text{-}191}$ or $apoE_{1\text{-}231}$. In contrast to the N-terminal truncation, C-terminal truncation of apoE3 and apoE4 proteins did not induce any significant variation. On the other hand, apoE C-terminal domain seemed to play an important role in the protein self-association of both apoE3 and apoE4.

Choy et al. (2004) suggested that there is an intermolecular coiled-coil formation in the apoE C-terminal domain. By sedimentation equilibrium studies, the dimer-tetramer-octamer model is suggested in the lipid-free environments, whereas the monomer-dimer-tetramer model is well maintained in the presence of 50% trifluoroethanol. Our sedimentation velocity studies showed that the only species present for the apoE C-terminal domain is a tetramer ($s = 3.0$) in PBS and the major species is a dimer ($s = 1.5$) in the presence of dihexanoylphosphatidylcholine (T. H. Lin, unpublished data).

The function of apoE to lower plasma cholesterol in vivo was checked by injection of proteins into apoE(−) mice (C. Y. Chou, G. G. Chang, and M. S. Shiao, unpublished

data). The functional assay showed that full-length and truncated apoE proteins were active in vivo. Animal studies were conducted using apoE isoform proteins in pairs. Our preliminary results indicate that full-length apoE3 and apoE4, $apoE3_{41\text{-}299}$, $apoE4_{41\text{-}299}$, and $apoE4_{72\text{-}299}$ lowered the plasma cholesterol to a similar extent. However, the efficacy of $apoE3_{72\text{-}299}$ was significantly lower than that of full-length or $apoE4_{72\text{-}299}$ (30% less). This correlates well with helix 2 in the N-terminus being involved in the LDL receptor binding, especially for apoE3. One possibility is that stabilization by helix 2 to the LDL receptor binding of apoE3 proteins is more important than that of two-domain interactions. The more stabilized apoE4 isoform, which may assist in the domain-domain interaction, is less affected by helix 2 truncation. Other stabilization interactions may exist beyond the interaction of Arg-61 with Glu-255 and these may stabilize an extended helical structure in the carboxyl terminus to accommodate a larger, less-curved VLDL surface (Dong and Weisgraber, 1996).

Huang et al. (2001) have shown that C-terminal truncated fragments of apoE4 (272–299 amino acids removed) is generated inside cultured neurons and in brains of AD patients and interacted with p-tau and p-NF-H, resulting in large, filamentous intracellular inclusions resembling NFT in AD brains. When residues 245–271 in the C-terminus is deleted, the ability of apoE4 to form intracellular inclusions is completely lost. They have also found that N-terminal truncated apoE4 (1–85 residues removed) induces more NFT in culture neurons. The higher aggregation tendency of N-terminal truncated apoE4 and the importance of the C-terminus (232–271) in the self-association observed in our study may be due to the same reason. The findings for structural variation in N-terminal truncated apoE3 and apoE4 provide useful information to explain the higher levels of aggregation of the E4 isoform and this supports the involvement of E4 in AD. Our studies thus provide a direction for the rational design of drugs that may inhibit the aggregation of apoE4 and targeting this may delay the formation of NFT or extracellular amyloid plaques.

We thank Shou-Hsing Wu, Wei-Ping Jen, and Jing-Jing Chiu for assistance with protein functional assay. The dynamic light scattering machine was kindly provided by Dr. Hanna S. Yuan of the Institute of Molecular Biology, Academia Sinica, Taipei, Taiwan. We thank Wei-Jen Yang for technical assistance with the dynamic light scattering experiments. We also thank Prof. Liang Tong (Dept. of Biological Sciences, Columbia University, New York) for advice during the course of this research.

This work was supported by the program for Promoting University Academic Excellence, National Science Council, and Taipei Veterans General Hospital, Taiwan, Republic of China.

REFERENCES

Andrade, M. A., P. Chacon, J. J. Merelo, and F. Moran. 1993. Evaluation of secondary structure of proteins from UV circular dichroism using an unsupervised learning neural network. *Protein Eng.* 6:383–390.

Baldwin, R. L. 1953. Sedimentation coefficients of small molecules: methods of measurement based on the refractive-index gradient curve. The sedimentation coefficient of polyglucose A. *Biochem. J.* 55:644–648.

Braman, J., C. Papworth, and A. Greener. 1996. Site-directed mutagenesis using double-stranded plasmid DNA templates. *Methods Mol. Biol.* 57: 31–44.

Chauhan, N. B. 2003. Membrane dynamics, cholesterol homeostasis, and Alzheimer's disease. *J. Lipid Res.* 44:2019–2029.

Choy, N., V. Raussens, and V. Narayanaswami. 2004. Inter-molecular coiled-coil formation in human apolipoprotein E C-terminal domain. *J. Mol. Biol.* 334:527–539.

Cox, D. J. 1969. Computer simulation of sedimentation in the ultracentrifuge. IV. Velocity sedimentation of self-associating solutes. *Arch. Biochem. Biophys.* 129:106–123.

Demant, T., D. Bedford, C. J. Packard, and J. Shepherd. 1991. Influence of apolipoprotein E polymorphism on apolipoprotein B-100 metabolism in normolipemic subjects. *J. Clin. Invest.* 88:1490–1501.

De Pauw, M., B. Vanloo, A. D. Dergunov, A. M. Devreese, J. Baert, R. Brasseur, and M. Rosseneu. 1997. Composition and structural and functional properties of discoidal and spherical phospholipid-apoE3 complexes. *Biochemistry (Mosc.).* 62:251–263.

Dong, L. M., and K. H. Weisgraber. 1996. Human apolipoprotein E4 domain interaction. Arginine 61 and glutamic acid 255 interact to direct the preference for very low density lipoproteins. *J. Biol. Chem.* 271: 19053–19057.

Dong, L. M., C. Wilson, M. R. Wardell, T. Simmons, R. W. Mahley, K. H. Weisgraber, and D. A. Agard. 1994. Human apolipoprotein E. Role of arginine 61 in mediating the lipoprotein preferences of the E3 and E4 isoforms. *J. Biol. Chem.* 269:22358–22365.

Fan, D. D., Q. Q. Li, L. Korando, W. Gray Jerome, and J. J. Wang. 2004. A monomeric human apolipoprotein E carboxyl-terminal domain. *Biochemistry.* 43:5055–5064.

Farkas, M. H., K. H. Weisgraber, V. L. Shepherd, M. F. Linton, S. Fazio, and L. L. Swift. 2004. The recycling of apolipoprotein E and its amino-terminal 22 kDa fragment: evidence for multiple redundant pathways. *J. Lipid Res.* 45:1546–1554.

Fujita, H. 1975. Foundations of Ultracentrifugal Analysis. Wiley, New York.

Gearing, M., G. W. Rebeck, B. T. Hyman, J. Tigges, and S. S. Mirra. 1994. Neuropathology and apolipoprotein E profile of aged chimpanzees: implications for Alzheimer disease. *Proc. Natl. Acad. Sci. USA.* 91: 9382–9386.

Harris, F. M., W. J. Brecht, Q. Xu, I. Tesseur, L. Kekonius, T. Wyss-Coray, J. D. Fish, E. Masliah, P. C. Hopkins, K. Scearce-Levie, K. H. Weisgraber, L. Mucke, R. W. Mahley, and Y. Huang. 2003. Carboxyl-terminal-truncated apolipoprotein E4 causes Alzheimer's disease-like neurodegeneration and behavioral deficits in transgenic mice. *Proc. Natl. Acad. Sci. USA.* 100:10966–10971.

Henderson, A. S., S. Easteal, A. F. Jorm, A. J. Mackinnon, A. E. Korten, H. Christensen, L. Croft, and P. A. Jacomb. 1995. Apolipoprotein E allele epsilon 4, dementia, and cognitive decline in a population sample. *Lancet.* 346:1387–1390.

Huang, Y., X. Q. Liu, T. Wyss-Coray, W. J. Brecht, D. A. Sanan, and R. W. Mahley. 2001. Apolipoprotein E fragments present in Alzheimer's disease brains induce neurofibrillary tangle-like intracellular inclusions in neurons. *Proc. Natl. Acad. Sci. USA.* 98:8838–8843.

Kao, J. T., K. S. Tsai, C. J. Chang, and P. C. Huang. 1995. The effects of apolipoprotein E polymorphism on the distribution of lipids and lipoproteins in the Chinese population. *Atherosclerosis.* 114:55–59.

Lalazar, A., and R. W. Mahley. 1989. Human apolipoprotein E. Receptor binding activity of truncated variants with carboxyl-terminal deletions. *J. Biol. Chem.* 264:8447–8450.

Lamm, O. 1929. Die differentialgleichung der ultrazentrifugierung. *Ark. Mat. Astr. Fys.* 21B:1–4.

Laue, T. M., B. D. Shah, T. M. Ridgeway, and S. L. Pelletier. 1992. Computer-aided interpretation of analytical sedimentation data for proteins. *In* Analytical Ultracentrifugation in Biochemistry and Polymer Science. S. E. Harding, A. J. Rowe, and J. C. Horton, editors. The Royal Society of Chemistry, Cambridge, UK. 90–125.

Li, X. P., K. Kypreos, E. E. Zanni, and V. Zannis. 2003. Domains of apoE required for binding to apoE receptor 2 and to phospholipids: Implication for the functions of apoE in the brain. *Biochemistry*. 42:10406–10417.

Lobley, A., and B. A. Wallace. 2001. A website for the analysis of protein secondary structure from circular dichroism spectra. *Biophys. J*. 80:373 (Abstr.).

Lobley, A., L. Whitmore, and B. A. Wallace. 2002. DICHROWEB: an interactive website for the analysis of protein secondary structure from circular dichroism spectra. *Bioinformatics*. 18:211–212.

Marx, J. 1993. Alzheimer's pathology begins to yield its secrets. *Science*. 259:457–458.

Morrow, J. A., D. M. Hatters, B. Lu, P. Hochtl, K. A. Oberg, B. Rupp, and K. H. Weisgraber. 2002. Apolipoprotein E4 forms a molten globule. A potential basis for its association with disease. *J. Biol. Chem*. 277:50380–50385.

Nathan, B. P., S. Bellosta, D. A. Sanan, K. H. Weisgraber, R. W. Mahley, and R. E. Pitas. 1994. Differential effects of apolipoproteins E3 and E4 on neuronal growth in vitro. *Science*. 264:850–852.

Pericak-Vance, M. A., and J. L. Haines. 1995. Genetic susceptibility to Alzheimer disease. *Trends Genet*. 11:504–508.

Perugini, M. A., P. Schuck, and G. J. Howlett. 2000. Self-association of human apolipoprotein E3 and E4 in the presence and absence of phospholipid. *J. Biol. Chem*. 275:36758–36765.

Polvikoski, T., R. Sulkava, M. Haltia, K. Kainulainen, A. Vuorio, A. Verkkoniemi, L. Niinisto, P. Halonen, and K. Kontula. 1995. Apolipoprotein E, dementia, and cortical deposition of beta-amyloid protein. *N. Engl. J. Med*. 333:1242–1247.

Provencher, S. W., and J. Glockner. 1981. Estimation of globular protein secondary structure from circular dichroism. *Biochemistry*. 20:33–37.

Raffai, R. L., and K. H. Weisgraber. 2003. Cholesterol: from heart attacks to Alzheimer's disease. *J. Lipid Res*. 44:1423–1430.

Rogers, D. P., C. G. Brouillette, J. A. Engler, S. W. Tendian, L. Roberts, V. K. Mishra, G. M. Anantharamaiah, S. Lund-Katz, M. C. Phillips, and M. J. Ray. 1997. Truncation of the amino terminus of human apolipoprotein A-I substantially alters only the lipid-free conformation. *Biochemistry*. 36:288–300.

Saito, H., P. Dhanasekaran, F. Baldwin, K. H. Weisgraber, S. Lund-Katz, and M. C. Phillips. 2001. Lipid binding-induced conformational change in human apolipoprotein E. Evidence for two lipid-bound states on spherical particles. *J. Biol. Chem*. 276:40949–40954.

Saito, H., P. Dhanasekaran, F. Baldwin, K. H. Weisgraber, M. C. Phillips, and S. Lund-Katz. 2003. Effects of polymorphism on the lipid interaction of human apolipoprotein E. *J. Biol. Chem*. 278:40723–40729.

Sanan, D. A., K. H. Weisgraber, S. J. Russell, R. W. Mahley, D. Huang, A. Saunders, D. Schmechel, T. Wisniewski, B. Frangione, A. D. Roses, and W. J. Strittmatter. 1994. Apolipoprotein E associates with beta amyloid peptide of Alzheimer's disease to form novel monofibrils. Isoform apoE4 associates more efficiently than apoE3. *J. Clin. Invest*. 94:860–869.

Sánchez del Pino, M. M., and A. R. Fersht. 1997. Nonsequential unfolding of the alpha/beta barrel protein indole-3-glycerol-phosphate synthase. *Biochemistry*. 36:5560–5565.

Schellenberg, G. D. 1995. Genetic dissection of Alzheimer disease, a heterogeneous disorder. *Proc. Natl. Acad. Sci. USA*. 92:8552–8559.

Schuck, P. 1998. Sedimentation analysis of noninteracting and self-associating solutes using numerical solutions to the Lamm equation. *Biophys. J*. 75:1503–1512.

Schuck, P. 2000. Size-distribution analysis of macromolecules by sedimentation velocity ultracentrifugation and Lamm equation modeling. *Biophys. J*. 78:1606–1619.

Schuck, P. 2003. On the analysis of protein self-association by sedimentation velocity analytical ultracentrifugation. *Anal. Biochem*. 320:104–124.

Schuck, P., M. A. Perugini, N. R. Gonzales, G. J. Howlett, and D. Schubert. 2002. Size-distribution analysis of proteins by analytical ultracentrifugation: strategies and application to model systems. *Biophys. J*. 82:1096–1111.

Selkoe, D. J. 2001. Alzheimer's disease: genes, proteins, and therapy. *Physiol. Rev*. 81:741–766.

Semisotnov, G. V., N. A. Rodionova, O. I. Razgulyaev, V. N. Uversky, A. F. Gripas, and R. I. Gilmanshin. 1991. Study of the ''molten globule'' intermediate state in protein folding by a hydrophobic fluorescent probe. *Biopolymers*. 31:119–128.

Siest, G., T. Pillot, A. Regis-Bailly, B. Leininger-Muller, J. Steinmetz, M. M. Galteau, and S. Visvikis. 1995. Apolipoprotein E: an important gene and protein to follow in laboratory medicine. *Clin. Chem*. 41:1068–1086.

Solovyova, A., P. Schuck, L. Costenaro, and C. Ebel. 2001. Non-ideality by sedimentation velocity of halophilic malate dehydrogenase in complex solvents. *Biophys. J*. 81:1868–1880.

Sreerama, N., S. Y. Venyaminov, and R. W. Woody. 1999. Estimation of the number of helical and strand segments in proteins using CD spectroscopy. *Protein Sci*. 8:370–380.

Sreerama, N., and R. W. Woody. 1993. A self-consistent method for the analysis of protein secondary structure from circular dichroism. *Anal. Biochem*. 209:32–44.

Strittmatter, W. J., and A. D. Roses. 1995. Apolipoprotein E and Alzheimer disease. *Proc. Natl. Acad. Sci. USA*. 92:4725–4727.

Van Bockxmeer, F. M., C. D. S. Mamotte, F. R. Gibbons, and R. R. Taylor. 1994. Apolipoprotein epsilon 4 homozygosity: a determinant of restenosis after coronary angioplasty. *Atherosclerosis*. 110:195–202.

Van Stokkum, I. H. M., H. J. W. Spoelder, M. Bloemendal, R. Van Grondelle, and F. C. A. Groen. 1990. Estimation of protein secondary structure and error analysis from CD spectra. *Anal. Biochem*. 191:110–118.

Weisgraber, K. H. 1994. Apolipoprotein E: structure-function relationships. *Adv. Protein Chem*. 45:249–302.

Westerlund, J. A., and K. H. Weisgraber. 1993. Discrete carboxyl-terminal segments of apolipoprotein E mediate lipoprotein association and protein oligomerization. *J. Biol. Chem*. 268:15745–15750.

Wilson, C., M. R. Wardell, K. H. Weisgraber, R. W. Mahley, and D. A. Agard. 1991. Three-dimensional structure of the LDL receptor-binding domain of human apolipoprotein E. *Science*. 252:1817–1822.